BRAIN-be 2.0

BELGIAN RESEARCH ACTION THROUGH INTERDISCIPLINARY NETWORKS - Phase 2

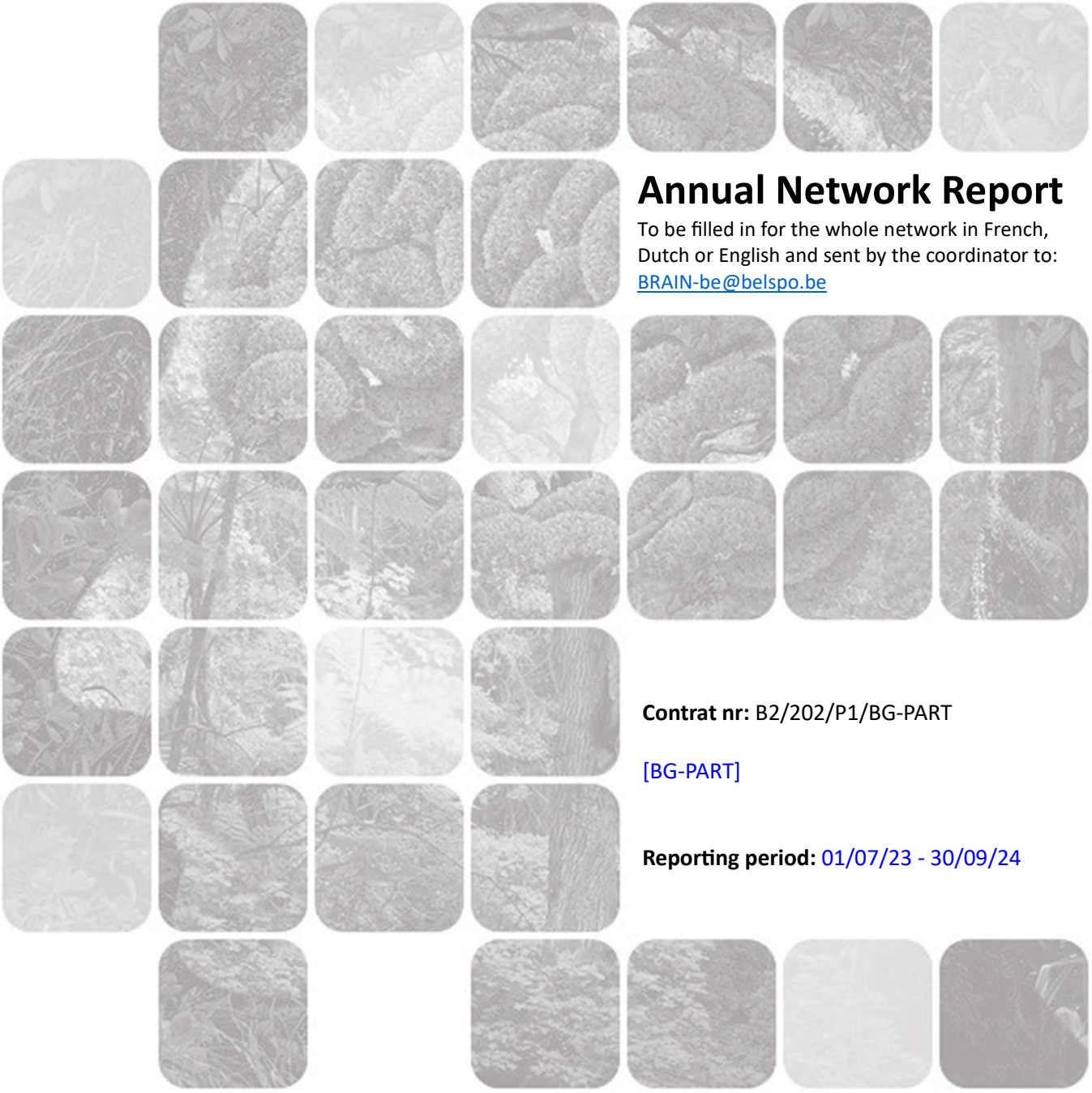

Annual Network Report

To be filled in for the whole network in French, Dutch or English and sent by the coordinator to: BRAIN-be@belspo.be

Contrat nr: B2/202/P1/BG-PART

[BG-PART]

Reporting period: 01/07/23 - 30/09/24

BRAIN-be 2.0 Annual Network Report

Third Annual Report completed on October 8, 2024

Project BG-PART

Project number: B2/202/P1/BG-PART

BioGeochemical PARTicle interactions and feedback loops on the Belgian Continental Shelf

Years 2021-2025

Network

Xavier Desmit, Nathan Terseleer, Michael Fettweis (RBINS)
Auria Kallend , Koen Sabbe, Wim Vyverman (PAE-Ugent)
Jens Dujardin, Maarten De Rijcke (VLIZ)

Citation

Desmit, X., Dujardin, J., Kallend, A., Terseleer, N., De Rijcke, M., Sabbe, K., Fettweis, M., 2024. BioGeochemical PARTicle interactions and feedback loops on the Belgian Continental Shelf, 3rd Annual Report. RBINS, Brussels.

Foreword

From the very beginning of BG-PART, the transdisciplinary nature of the project has been a challenge that we have systematically addressed through physical meetings and online interactions. The international workshop in Brussels in October 2023 marked the beginning of an increased collaboration between the principal investigators and our international colleagues (incl. from the Follow-Up Committee). By the end of the third year of this 4-year project, we have gathered a substantial amount of original data, which we plan to analyze in the coming months. This report illustrates the type of data we aim to manipulate to answer the project's questions.

Executive Summary

The fundamental question of the project is to elucidate the fine interactions between planktonic organisms, marine gels and mineral sediments along the coastal-offshore gradient of a turbid and tidal system. Our approach included monthly in situ samplings along the gradient (coupled with continuous sampling at MOW1 and remote sensing), laboratory experiments (including phytoplankton niche characterization and flocculation experiments), and numerical modeling of phytoplankton-sediment interactions.

In the last three years, some efforts have focused on the link between organic matter and mineral particles, and how these interactions influence the dynamics of suspended particles. Some papers have been published and, at this stage, we intend to study in more detail how these organo-mineral interactions fit into the marine carbon cycle.

Beyond the measured bulk organic matter, we aim to better identify the biological processes producing the biomass and marine gels responsible for organo-mineral interactions. This story starts with the characterization of phytoplankton and zooplankton species (from pico to micro size), and their seasonal succession. Although species assemblages vary each year, we are currently identifying their main seasonal patterns along the Belgian cross-shore gradient.

Laboratory experiments have allowed characterizing not only the niche of different dominant phytoplankton species, but also their capacity to produce and excrete exopolymeric substances under variable conditions. Measurements performed in an incubator are now available and describe the production of polysaccharides, Transparent Exopolymeric Particles (TEP), and Coomassie Stainable Particles (CSP).

These results – and the substantial amount of underlying data – will be further analyzed in the coming months to draw general lines explaining the dynamics we observed in the natural system. To this end, we also use numerical modeling to simulate the fine interactions between phytoplankton, marine gels and mineral particles undergoing flocculation in a theoretical water column. The approach and first outputs of the model are presented in this report.

With our datasets, we have gained useful insights into the dynamics of the natural system during the first three years. Our challenge during this last year is to interpret this data and produce a new set of transdisciplinary, original and useful hypotheses for the scientific community.

Table of Content

1. Achieved Work

1.1. Quantifying the organic carbon associated to suspended mineral particles in shelf seas

1.1.1. Introduction

Organic carbon associates with suspended clay particles in the marine system by adsorbing onto their mineral surfaces (Keil et al., 1994). This interaction stabilizes organic carbon, slowing or preventing further degradation, whether the organic matter is intrinsically labile or not (Hemingway et al., 2019; Kleber et al., 2021). Such organo-mineral association accounts for a major carbon sink in land soils and marine sediments, controlling the long-term balance of oxygen and carbon dioxide in the atmosphere. Particles and associated organic carbon flow from rivers or from cliff erosion into the sea (Dobrynin, 2009; Fettweis et al., 2007). Unless it has been processed already in the upstream estuary, most of this terrestrial organic matter is stripped from its mineral matrix and efficiently degraded in the receiving marine system, which explains why terrestrial organic carbon is proportionally lesser in marine sediment or dissolved pools than expected from river loads (Hedges et al., 1997). Through the adsorption/desorption kinetics, the mineral-associated terrestrial organic carbon can be replaced by organic carbon from marine origin, although that exchange dynamic depends on the mineralogical composition of the phyllosilicates (Blattmann et al., 2019). Clay particles are eroded from continental or marine deposits and journey throughout marginal seas, while being subject to continuous settling and resuspension cycles at tidal to seasonal scales (Fettweis et al., 2022). The suspended clays can be seen as a reservoir of particles hosting and transporting preserved organic carbon. In sediments, the preservation of organic carbon relies on the opposition between protection via mineral interactions and degradation processes, whether heterotrophic metabolism or abiotic redox and oxidative degradation (Keil & Mayer, 2014; Kleber et al., 2021). In marginal seas, organic carbon accumulates in surficial seabed sediments at a rate of approximately 0.126–0.350 Pg per year (Keil, 2017). At the scale of the global ocean, the accumulation of organic carbon in sediment constitutes a standing stock of the order of 87 ± 43 Pg in the top 5 cm of oceanic sediment (Lee et al., 2019) and 2322 Pg in the top meter (Atwood et al., 2020). While estimates of seafloor carbon stocks are underway at local and global scales, the stock of organic carbon associated with mineral particles suspended in the water column remains poorly understood. Yet, it reflects a sink of carbon, and the dynamics of suspended particles influence the distribution and accumulation patterns of associated organic carbon in the marine environment. Here, we provide an estimate of the stock and fluxes of mineral-associated organic carbon suspended on average in the water column across the North Sea shelf.

1.1.2. Methods

Our methodology combines monthly satellite products of surface SPM concentrations, in situ records of vertical profiles of SPM concentration, and a model estimate of the mineral-associated POC.

1. **Satellite product of surface SPMC**: this provides monthly SPM concentrations at the sea surface (Sentinel-3 and OLCI resolution, atmosphere algorithms, water color to SPMC algorithm, *possibly DINEOF?*, validation is provided by D. Van der Zande)
2. **In situ SPMC vertical profile** (tidal averaged): data from Belgian monitoring campaigns and from the German monitoring campaigns (ScanFish) allow calculating tidal averaged vertical profiles of SPM concentration from shallow turbid to stratified areas in the North Sea. When

the vertical profiles are expressed as exponential functions, we use this simple model to integrate SPM concentration on the vertical. Otherwise, we use a ratio between sea surface SPM concentration and the vertical averaged SPM concentration.

3. **Diagnostic model of POC:SPM content**: the diagnostic model of Schartau et al. (2019) allows estimating the mineral-associated POC concentration as a function of SPM concentration. However, this approach is subject to the fitting assumptions of the diagnostic model. Another estimate of the mineral-associated POC will be made at a later stage based on the mineralogy of SPM (see Fettweis et al., subm.)

1.1.3. Results and Discussion

Surface concentrations of suspended particulate matter (SPM) can be estimated with remote sensing from Sentinel-3, providing reliable monthly averages (Fig.1; see Methods for details).

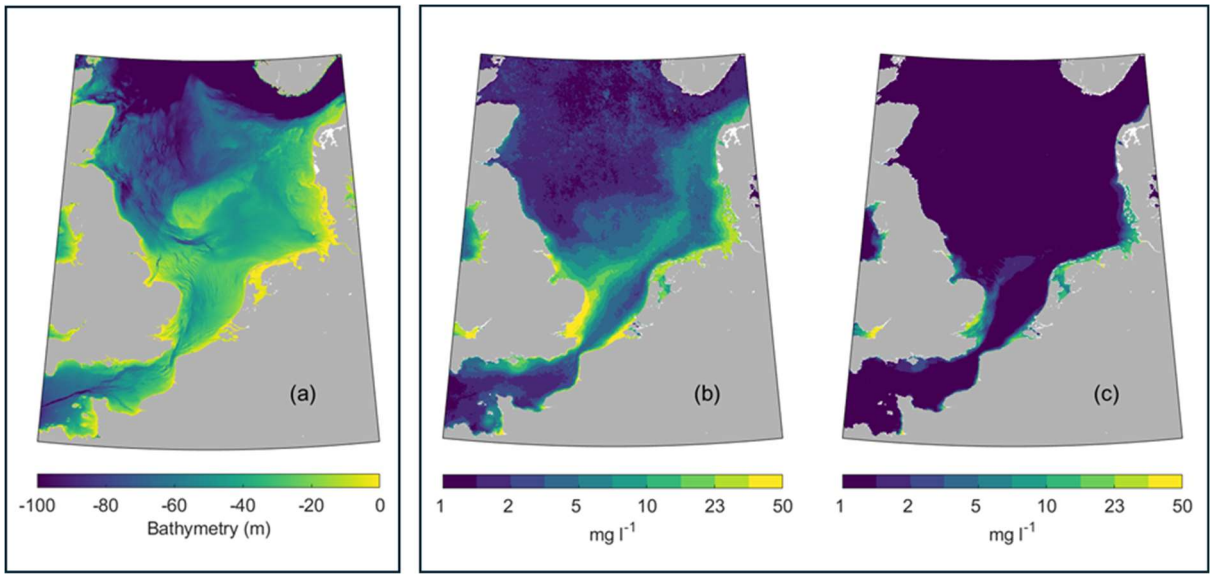

Figure 1 (a) Bathymetry in the studied domain of the North Sea shelf (data: GEBCO); (b) surface SPM concentration in winter (Dec, Jan, Feb) and (c) summer (Jun, Jul, Aug) in 2021 (data: Sentinel-3, OLCI sensor).

The extrapolation of surface SPM concentrations throughout the entire water column is done with vertical profiles measured in situ at an hourly frequency and averaged over a tidal cycle (Fig.2). Though the lambda parameter of the exponential increase of SPM concentration on the vertical varies with the tide, it is quite stable on a seasonal average in our well mixed water column. Note that other data collected in the German Bight (ScanFish) must still be analyzed to provide a better estimate of vertically-integrated SPM concentration in stratified areas (not done for this report).

The typical decrease of the SPM concentration between winter and summer is featured on these graphs at both the top and the bottom end-members of the water column. Such seasonal decrease is due to the enhanced flocculation of particles in the summer following the accumulation in the water column of sticky exopolymeric substances excreted during the phytoplankton bloom (Fettweis et al., 2022).

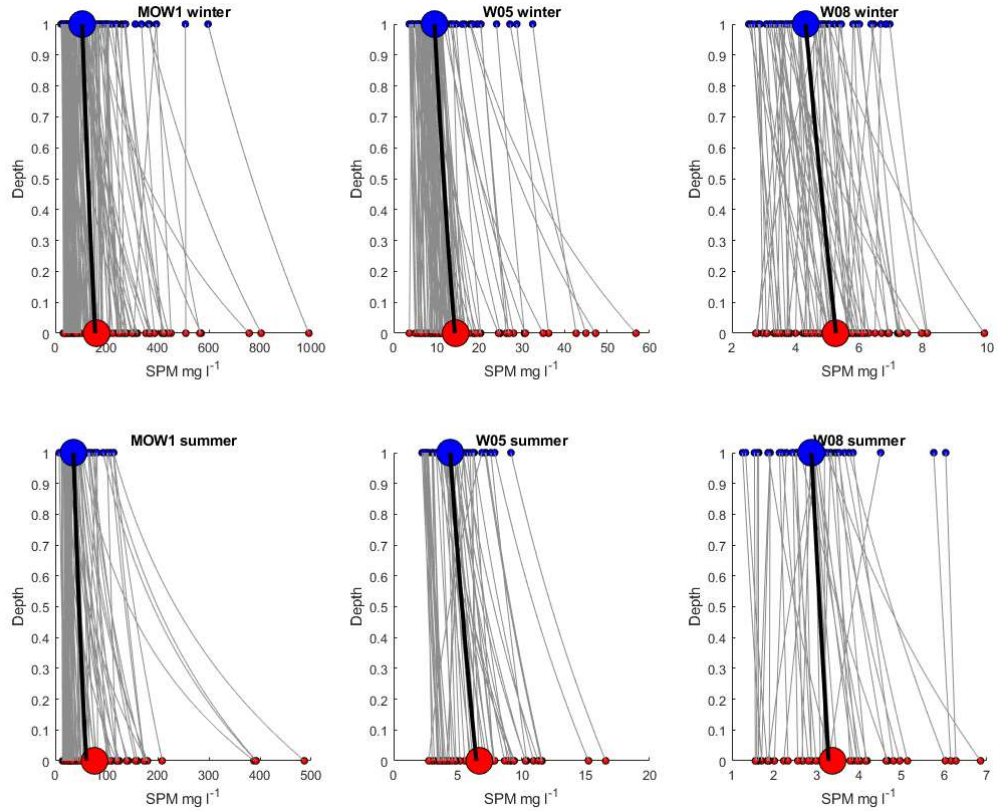

Figure 2 Surface (blue) and bottom (red) SPM concentrations (in situ observations) with their calculated exponential vertical increase (grey lines) during several tidal cycles (hourly samplings) at three stations along the Belgian cross-shore axis and during two seasons (winter, top, and summer, bottom). Larger dots and black lines show the average values per station and per season.

The calculation of the vertical profiles of SPM concentration is subject to several assumptions. Firstly, observing that turbid coastal and clear offshore waters exhibit different particle composition and dynamics (Fettweis et al., subm.), we assume that such inshore-offshore distinction is the most relevant feature explaining the vertical profiles of SPM concentrations on the shelf sea. Thus, we assume that the vertical profiles measured along the Belgian cross-shore gradient of SPM concentrations can be used everywhere else as long as the water masses are classified between coastal and offshore systems with respect to particle dynamics (as, for instance, in Desmit et al., 2024). Secondly, we assume that the monthly-averaged surface SPM concentration delivered by the satellite is also a tidal averaged concentration in each pixel. Hence, we use a tidal-averaged vertical profile of SPM concentration. Thirdly, we assume that the seasonally stratified waters exhibit vertical profiles of SPM concentrations similar to the non-stratified offshore waters where we made our observations [this is not correct and must be refined using ScanFish data]. These assumptions allow estimating grossly the monthly mass of SPM in the water column corresponding to each pixel of a monthly satellite image. The last step is to convert the SPM mass thus obtained into a mineral-associated organic carbon mass, which can be done with the diagnostic model of Schartau et al. (2019) and Fettweis et al. (2022). The diagnostic model reproduces the cross-shore gradient of the particulate organic carbon (POC) content of SPM as a function of the SPM concentration (Fig.3).

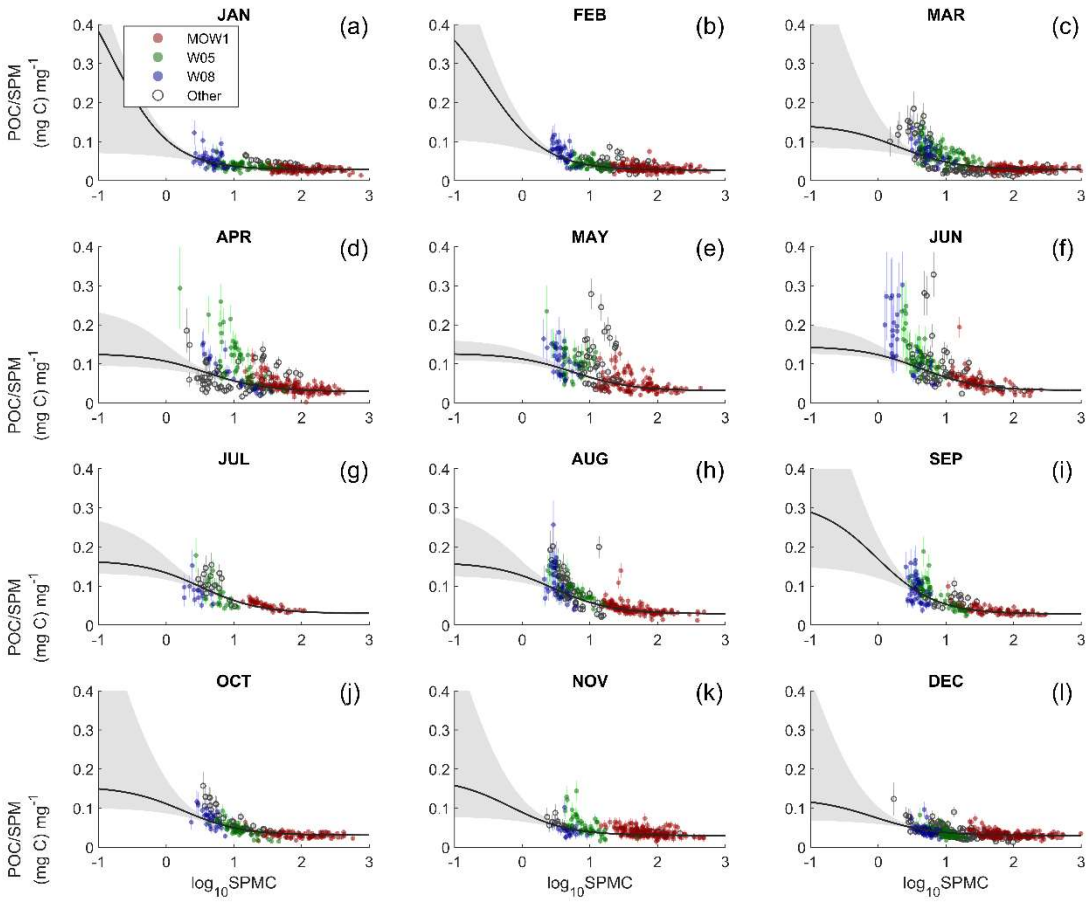

Figure 3 Monthly POC content of SPM as a function of SPM concentration. Dots depict observed values at sampling stations, line is the model fitting and grey areas are the 5% confidence intervals of the model.

More critically, the model is able to distinguish between the mineral-associated POC, considered more refractory, and the freshly produced POC, considered to be degraded at daily to monthly scales. In that step, we also assume that the monthly parameter coefficients obtained by fitting the model on observations collected along the Belgian cross-shore gradient can be used at any location elsewhere on the shelf sea. That assumption is supported by a previous comparison of model fitting on Belgian versus German Bight observations along the cross-shore gradient of SPM concentration. The total mass of the suspended mineral-associated POC in Winter is estimated close to ~0.003 Pg C on the North Sea shelf (see domain in Fig.1), which is equivalent on average to 5.8 10^{-9} Pg C/km^2. That amount is of the order of 2% of the carbon standing stock found on a global average in the first 5 cm of the ocean bed sediment (2.4 10^{-7} Pg C/km^2, adapted from Lee et al., 2019). The quantification of mineral-associated POC stock can be refined but will not significantly increase.

Based on previous works estimating the SPM loads from rivers entering the North Sea and the erosion of Suffolk and Holderness (Dobrynin, 2009), and the SPM net flux entering from the Channel (Fettweis et al., 2007), we estimated the total SPM flux entering the North Sea equal to ~40 10^6 ton yr^{-1}. This amount roughly corresponds to a flux of 0.001 Pg yr^{-1} of mineral-associated POC. This flux is comparable to the amount of mineral-associated POC in suspension on the North Sea shelf (0.003 Pg C), and it remains small compared to the fluxes of organic carbon accumulation on the seabed 0.126–0.350 Pg yr^{-1} (from Keil, 2017).

Literature

Atwood, T.B., Witt, A., Mayorga, J., Hammill, E., Sala, E., 2020. Global Patterns in Marine Sediment Carbon Stocks. Front. Mar. Sci. 7. https://doi.org/10.3389/fmars.2020.00165

Blattmann, T.M., Liu, Z., Zhang, Y., Zhao, Y., Haghipour, N., Montluçon, D.B., Plötze, M., Eglinton, T.I., 2019. Mineralogical control on the fate of continentally derived organic matter in the ocean. Science 366, 742–745. https://doi.org/10.1126/science.aax5345

Desmit, X., Schartau, M., Riethmüller, R., Terseleer, N., Van der Zande, D., Fettweis, M., 2024. The transition between coastal and offshore areas in the North Sea unraveled by suspended particle composition. Sci. Total Environ. 915, 169966. https://doi.org/10.1016/j.scitotenv.2024.169966

Dobrynin, M., 2009. Investigating the dynamics of suspended particulate matter in the North Sea using a hydrodynamic transport model and satellite data assimilation. Hamburg University, Hamburg. ISSN 0344-9629. https://www.hereon.de/imperia/md/content/hzg/zentrale_einrichtungen/bibliothek/berichte/2009/gkss_2009_12.pdf.

Fettweis, M., Nechad, B., Van den Eynde, D., 2007. An estimate of the suspended particulate matter (SPM) transport in the southern North Sea using SeaWiFS images, in situ measurements and numerical model results. Cont. Shelf Res. 27, 1568–1583. https://doi.org/10.1016/j.csr.2007.01.017

Fettweis, M., Schartau, M., Desmit, X., Lee, B.J., Terseleer, N., Van der Zande, D., Parmentier, K., Riethmüller, R., 2022. Organic Matter Composition of Biomineral Flocs and Its Influence on Suspended Particulate Matter Dynamics Along a Nearshore to Offshore Transect. J. Geophys. Res. Biogeosciences 127, e2021JG006332. https://doi.org/10.1029/2021JG006332

Fettweis, M., Silori, S., Adriaens, R., Desmit, X., (submitted). Clay minerals and the stability of organic carbon in suspension on the North Sea shelf. Geochim. Cosmochim. Acta.

Hedges, J.I., Keil, R.G., Benner, R., 1997. What happens to terrestrial organic matter in the ocean? Org. Geochem. 27, 195–212. https://doi.org/10.1016/S0146-6380(97)00066-1

Hemingway, J.D., Rothman, D.H., Grant, K.E., Rosengard, S.Z., Eglinton, T.I., Derry, L.A., Galy, V.V., 2019. Mineral protection regulates long-term global preservation of natural organic carbon. Nature 570, 228–231. https://doi.org/10.1038/s41586-019-1280-6

Keil, R., 2017. Anthropogenic Forcing of Carbonate and Organic Carbon Preservation in Marine Sediments. Annu. Rev. Mar. Sci. 9, 151–172. https://doi.org/10.1146/annurev-marine-010816-060724

Keil, R.G., Mayer, L.M., 2014. Mineral Matrices and Organic Matter (Chapter 12.12), in: Treatise on Geochemistry 2nd Edition. Elsevier Ltd., pp. 338–354.

Keil, R.G., Montluçon, D.B., Prahl, F.G., Hedges, J.I., 1994. Sorptive preservation of labile organic matter in marine sediments. Nature 370, 549–552. https://doi.org/10.1038/370549a0

Kleber, M., Bourg, I.C., Coward, E.K., Hansel, C.M., Myneni, S.C.B., Nunan, N., 2021. Dynamic interactions at the mineral–organic matter interface. Nat. Rev. Earth Environ. 2, 402–421. https://doi.org/10.1038/s43017-021-00162-y

Lee, T.R., Wood, W.T., Phrampus, B.J., 2019. A Machine Learning (kNN) Approach to Predicting Global Seafloor Total Organic Carbon. Glob. Biogeochem. Cycles 33, 37–46. https://doi.org/10.1029/2018GB005992

Schartau, M., Riethmüller, R., Flöser, G., van Beusekom, J.E.E., Krasemann, H., Hofmeister, R., Wirtz, K., 2019. On the separation between inorganic and organic fractions of suspended matter in a marine coastal environment. Prog. Oceanogr. 171, 231–250. https://doi.org/10.1016/j.pocean.2018.12.011

1.2. Phytoplankton and zooplankton succession on the Belgian continental shelf

We are close to determine the succession of phytoplankton species from picoplankton to microplankton by combining the data from different sources (under work). The following section mainly depicts the pico- and nanoplankton succession. It also provides information on the zooplankton species present at the Belgian stations throughout the year.

1.2.1. Phytoplankton from CytoSense flow cytometry

The CytoSense flow cytometer has been successfully deployed on 15 consecutive BG-PART campaigns, analyzing phytoplankton samples from surface and bottom waters between January 2022 and May 2023. This marks the longest uninterrupted period of use in the device's operational history (purchased in 2012), thanks to a decade of institutional experience and significant investment in preventative maintenance (multiple cleaning runs and frequent operation to prevent fouling and clogging). After checking, our cytometric data maintain high and consistent quality throughout the 18 months of BG-PART operations. Although the picture quality declined sharply after 6 months (likely due to camera misalignment caused by bumping during transport), the images were of secondary importance since the optical resolution is insufficient for accurate species description in the pico- and nanophytoplankton range we targeted (FlowCam or microscopy are superior for microphytoplankton).

In the last two years, we developed a new automated data processing pipeline for the CytoSense using a historical dataset. This pipeline automatically removes erroneous particles (electrical noise, fragments, bubbles, calibration beads) and irrelevant output variables, and calculates additional parameters, such as the ratios of each fluorescent signal and the ratio between forward and side scatter. We then applied a machine learning algorithm called Phenograph, initially developed for the medical sciences, to separate clusters in highly multidimensional flow cytometry data. Phenograph uses the k-nearest neighbor approach weighted by the Jaccard similarity coefficient and employs the Louvain method for rapid modularity optimization. This enables us to detect groups of cells with similar size, shape, density, and color ('cytometric clusters') within each sample. In a second step, we run the same Phenograph algorithm on the parameter means of each cluster found in all the samples to detect 'metaclusters', which are clusters present in one or more samples, thereby connecting our samples across depths, stations, and months. This is the first data pipeline for Cytosense data that allows us to intercompare clusters across samples. We can now track the relative and absolute density and biovolume of each metacluster across the entire BG-PART monitoring period. Additionally, the identification of metaclusters helps us describe the richness and composition of each sample, allowing us to identify different communities.

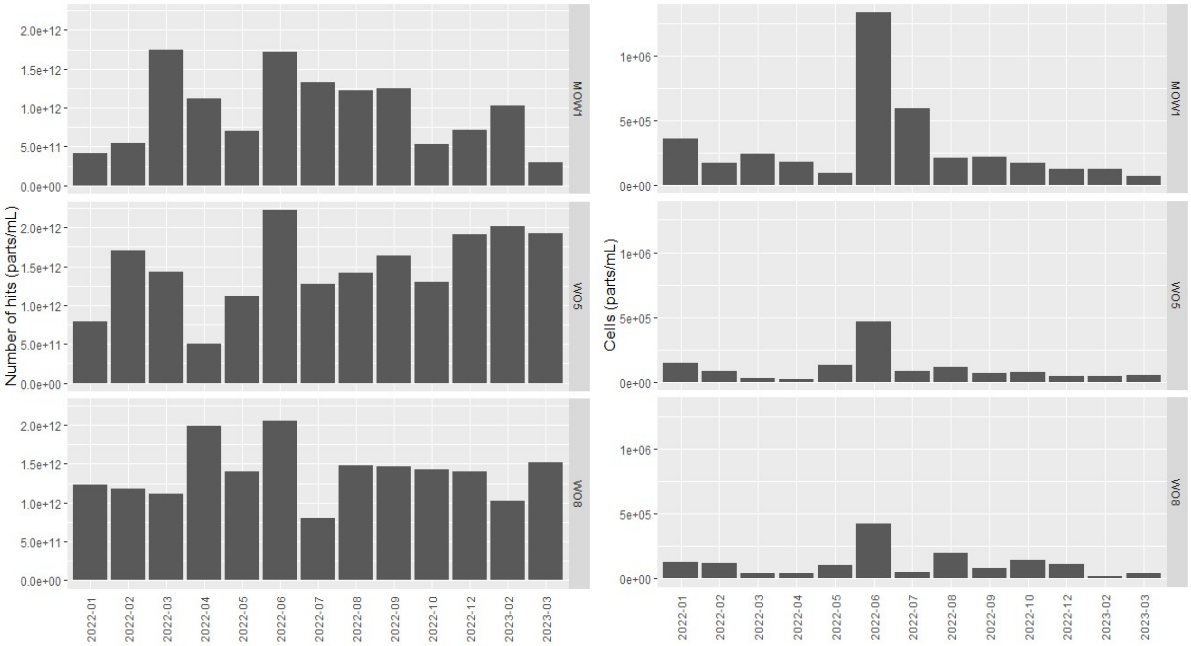

Figure 4: On the left: total number of "hits" the FCM detected as cytometric particle in the Nano to Pico size range. On the right: total concentration of cytometric particles present after the data clean-up step.

The newly developed pipeline significantly enhances the information we can extract from CytoSense flow cytometry, surpassing all other available tools for these data types (Fig.4). By implementing this approach, we go beyond the typical classification into functional groups (e.g., micro-, nano-, picophytoplankton). The downsides of this approach include the need to process and analyze the entire year's data simultaneously, causing lengthy calculation times for such a large dataset. The data pipeline has been applied on the entire BG-PART dataset.

We see in Figure 5 that the functional group "Pico red" dominates throughout the year. It is also evident from Figure 6 that there is a fairly consistent number of flow cytometric groups at each station during the sampling period. However, as seen in Figure 7, different flow cytometric groups comprise the community observed in Figure 6.

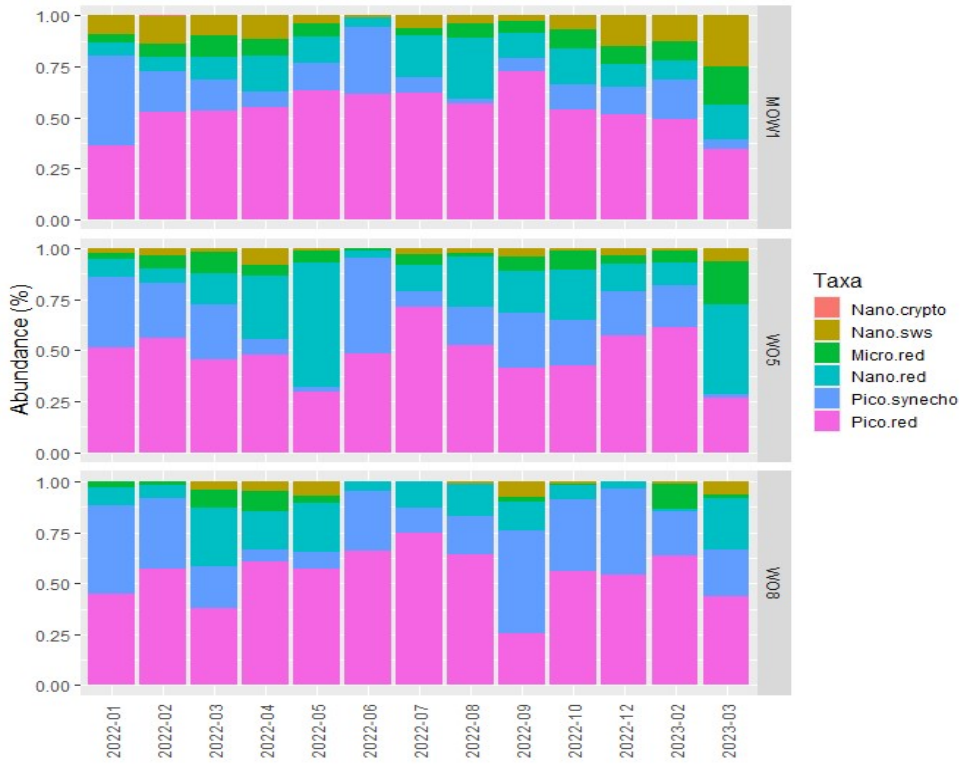

Figure 5: The relative abundance of cytometric functional groups at the three sampling stations, across the entire BG-PART sampling period. The acquisition protocol mainly targeted particles in the pico- to nano-size class.

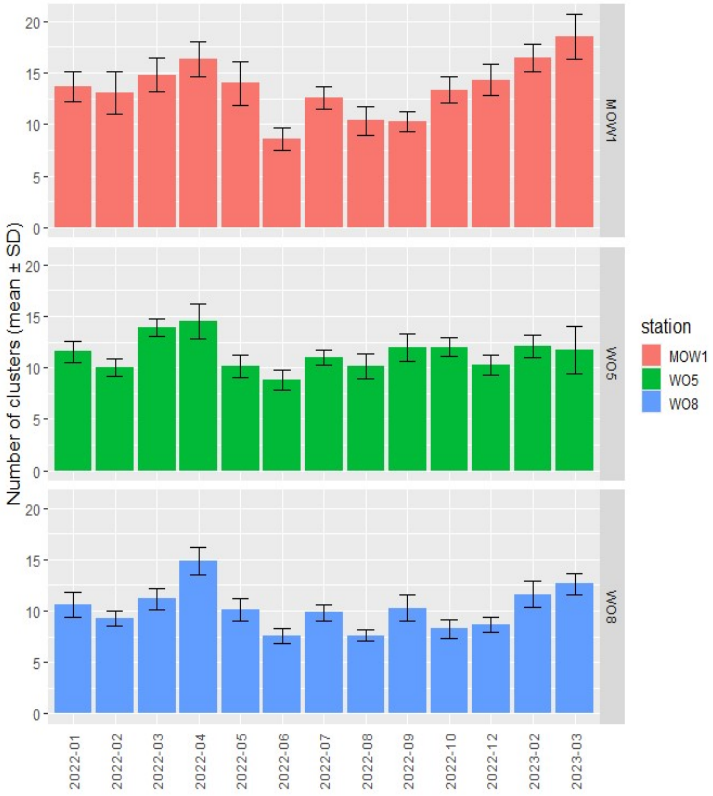

Figure 6: The total number of cytometric metaclusters present at each station throughout the sampling period. The nearshore diversity of nano- and picoplankton appears to be higher than the diversity further offshore.

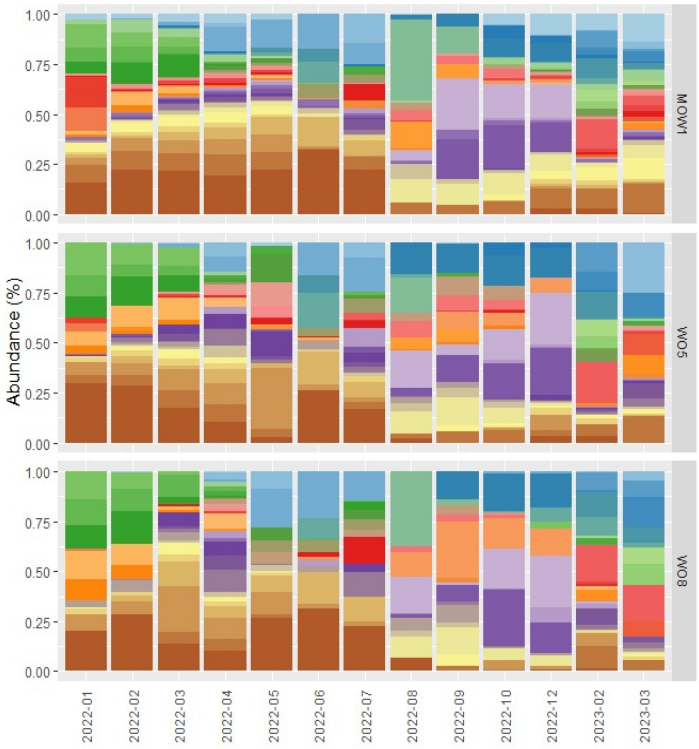

Figure 7: The relative abundance of individual cytometric metaclusters, revealing seasonal succession of pico- and nanoplanktonic cells at all three stations.

1.2.2. Zooplankton succession

Zooplankton samples were gathered using a WP2 vertical plankton net covering the entire water column at all stations when current speeds permitted deployment. 260 samples were collected and processed on a Zooscan using the protocol set in place by the LifeWatch Belgium project. The Zooscan produces individual pictures of particles from raw scans. The individual pictures, circa 800,000, produced from the BG-PART samples were annotated using the Ecotaxa platform through an algorithm trained on LifeWatch data from the Belgian part of the North Sea. The data was then individually checked by PhD student Jens Dujardin. This quality control step took several months. The data has recently been presented to the core team of the project and will be combined with the phytoplankton data to answer questions about the seasonality and tidal effects on the biota in the Belgian part of the North Sea. Furthermore, these data will be utilized to identify crucial zooplankton species for future experiments within the project.

Zooplankton grazing experiments have been postponed after the motorized plankton wheel we designed has proven to be too unwieldly for use within the climate rooms at VLIZ. This setup will be replaced with a simplified setup using Duran bottles wire-suspended in temperature-controlled water tanks. This setup will be easier to implement at VLIZ and was recently used at sea by the promotors of the project. While simpler, the approach is still considered to be suitable for the aim of investigating the consumption/consumption rate of marine gels by zooplankton.

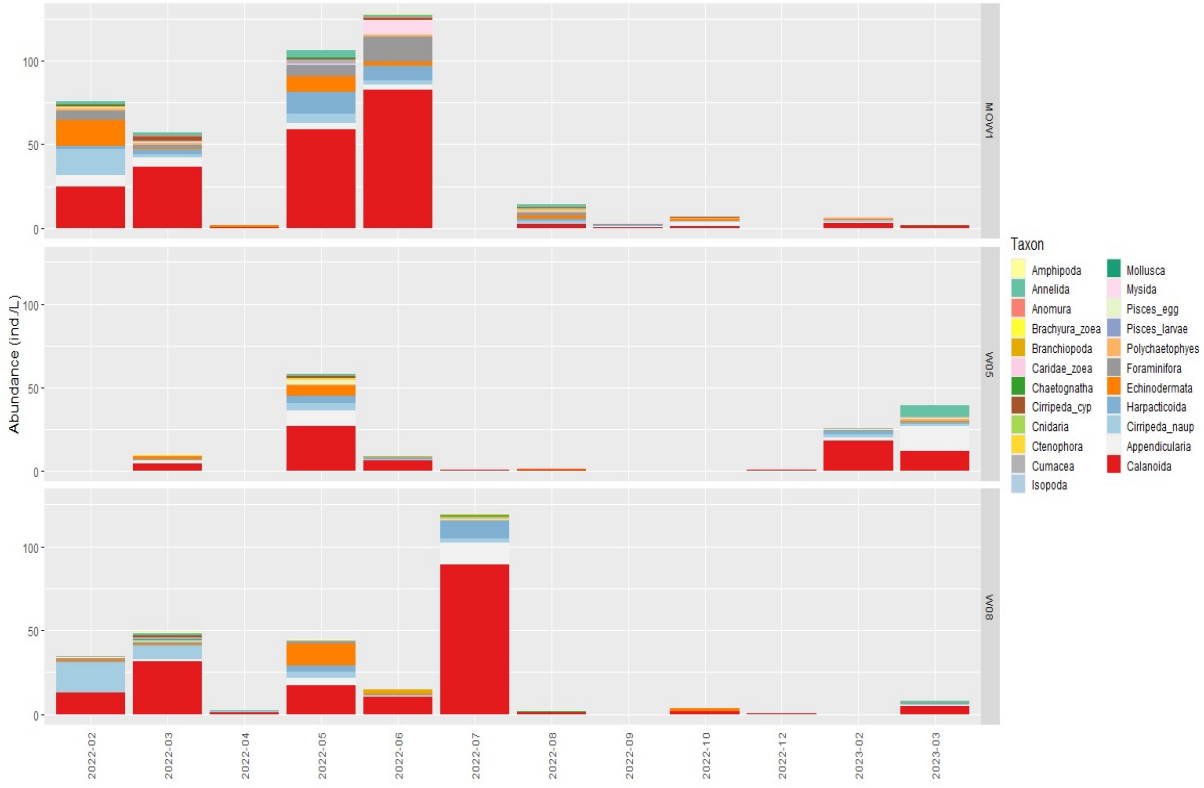

Figure 8: The total abundance of all zooplankton groups present at each station throughout the sampling period. Missing bars represent sampling days where the weather did not permit the safe deployment of the WP2-net.

Figure 8 shows the total abundance of zooplankton and suggests there were higher abundances in winter and early spring 2022 than in 2023. Zooplankton communities were mainly dominated by benthic (Harpacticoida) and pelagic (Calanoida) copepods, with the occasional occurrence of larval

stages (e.g. Echinodermata). Figure 9 furthermore reveals varying degrees of free-swimming tunicates (Appendicularia, also known as Larvaceans). Their importance in the North Sea ecosystem is less well defined than the copepods, though indiscriminate grazing on TEP particles has been previously described in literature (REF). Following these observations, copepods will be the organisms of focus in the planned grazing experiments. Amongst the copepods, the dominating group is Calanoida (Fig. 9 and 10), suggesting that there was not a significant disturbance of the sea bed, as Harpacticoida is closely associated with the sea bed. Figure 10 shows that during the year 2022, the dominance of copepods in certain months decreases while phytoplankton *Bellerochea* grows, especially in the coastal zone. *Bellerochea* is a genus of large, chain-forming diatoms that has recently appeared in large numbers in the LifeWatch long-term monitoring dataset. We hypothesize that shifts in summer temperatures are causing heat stress for the calanoid copepods, leading to predator release and summer blooms of this species.

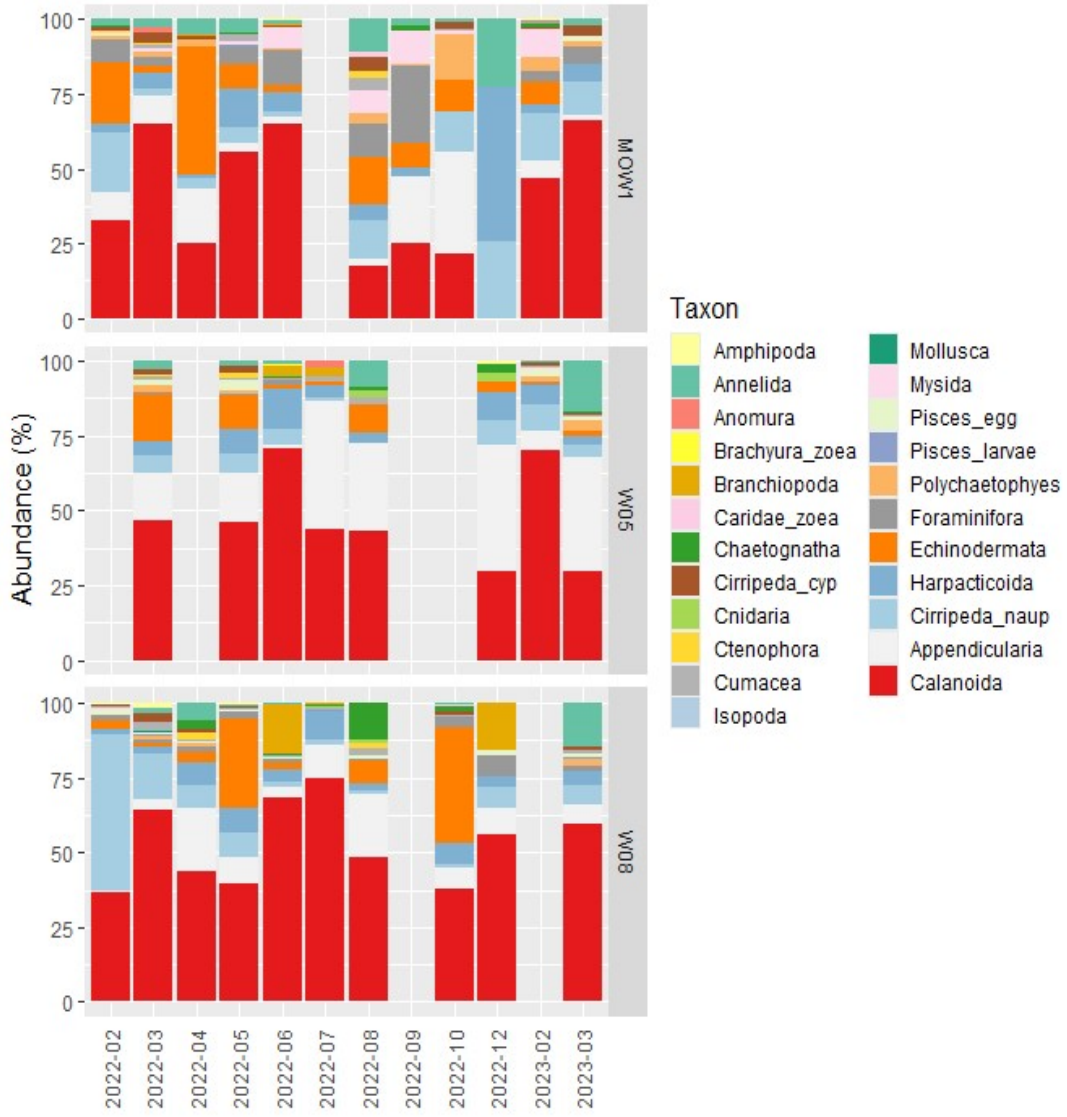

Figure 9: The relative abundance of the zooplankton groups present at each station throughout the sampling period.

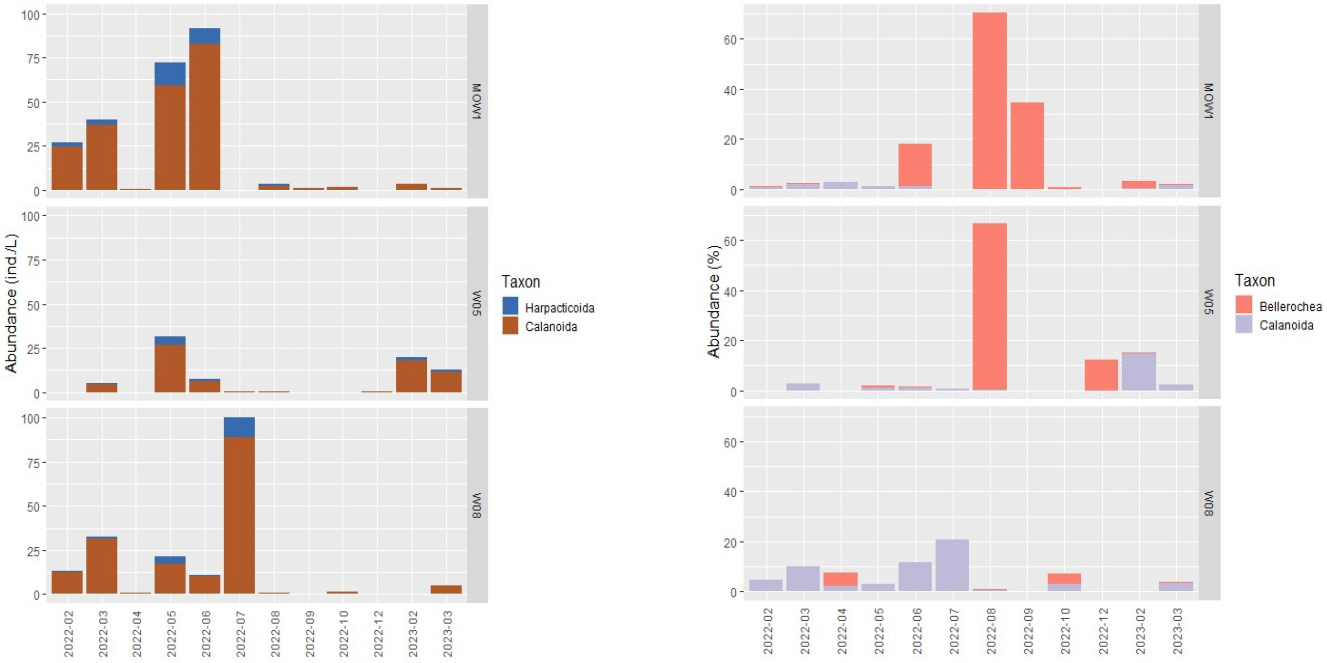

Figure 10: (left) The total number of the two copepod groups present at each station throughout the sampling period. The benthic Harpacticoida can be considered an indicator for the quality of sampling, as their presence signifies that a proper vertical transect was taken of the entire water column. (right) The relative abundance of Calanoida and Bellerochea at each station throughout the sampling period.

1.3. Particle composition and marine gel production by phytoplankton

1.3.1. Introduction

At the end of the winter/early spring in the Belgian part of the North Sea, the spring phytoplankton bloom is initiated by species that appear to be able to grow despite the low light (~high SPM and turbidity) and low temperature conditions. We hypothesize that these early bloom species produce marine gels that cause the SPM to aggregate, acting as a glue between the particles in the water column, thus forming bigger, denser particles that sink. This decrease in the SPM concentration would then allow for the more light demanding strains to grow.

1.3.2. Results

The FlowCam data (Fig.11) shows a more or less extended bloom of large phytoplankton (100-300 µm, i.e. large-celled phytoplankton and colonies/chains) at the coastal station M0W1, namely from spring to autumn (although with lower values in early summer), with a community mainly dominated by *Rhizosolenia* spp. and *Pseudo-nitzschia* spp. (spring-summer) and *Bellerochea* sp. (autumn). A single spring bloom was observed in the transition and offshore zones (respectively W05 and W08). The offshore community (W08) is dominated by *Rhizosolenia* spp., *Melosira* spp. and *Pseudo-nitzschia* spp., and the transition zone community (W05) shows mostly an intermediate of the two previous stations, but also presents some unique traits, such as the presence of *Guinardia* spp. The spring bloom in 2022 is larger than in 2023, which is also supported by the chlorophyll a data (taken by INS, Fig.12).

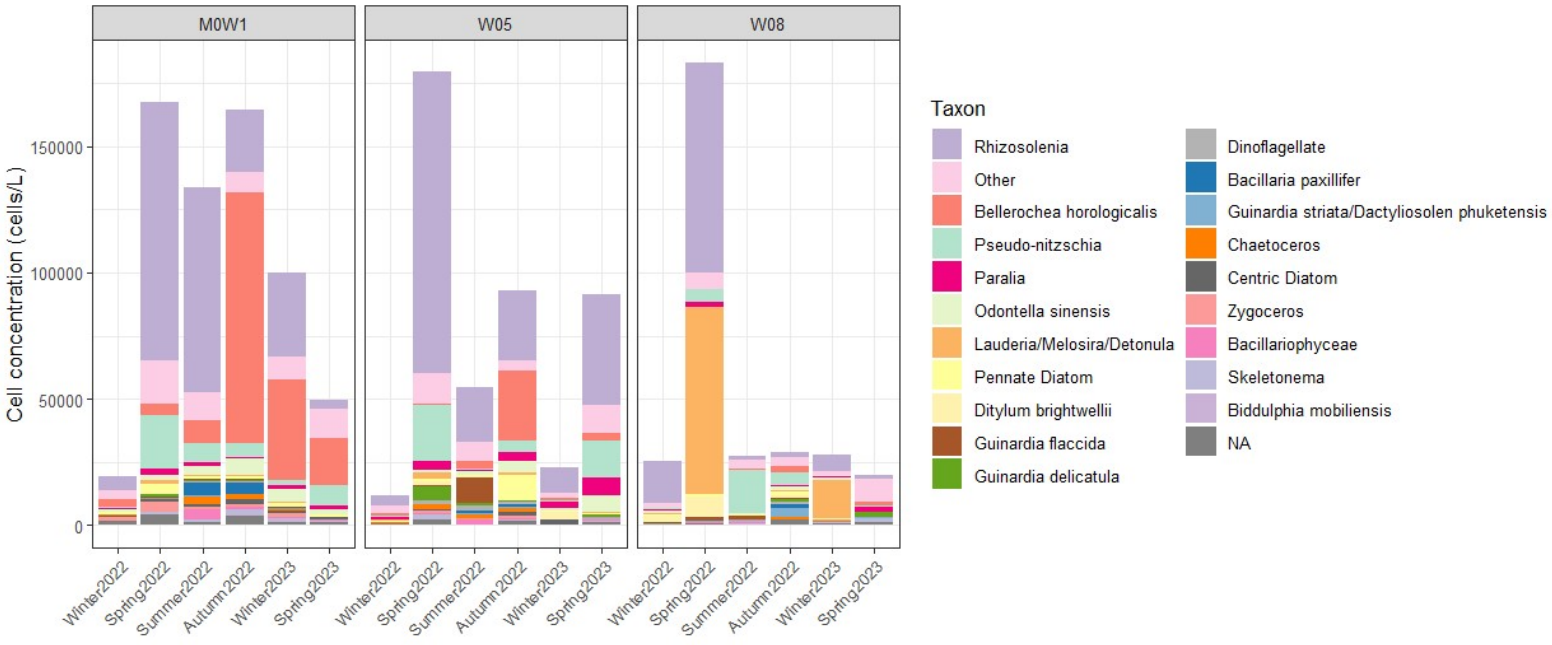

Figure 11: Large phytoplankton (100-300µm) community composition (FlowCam analysis) per season: top 20 most abundant genera. Red dashed line indicates the end of the year.

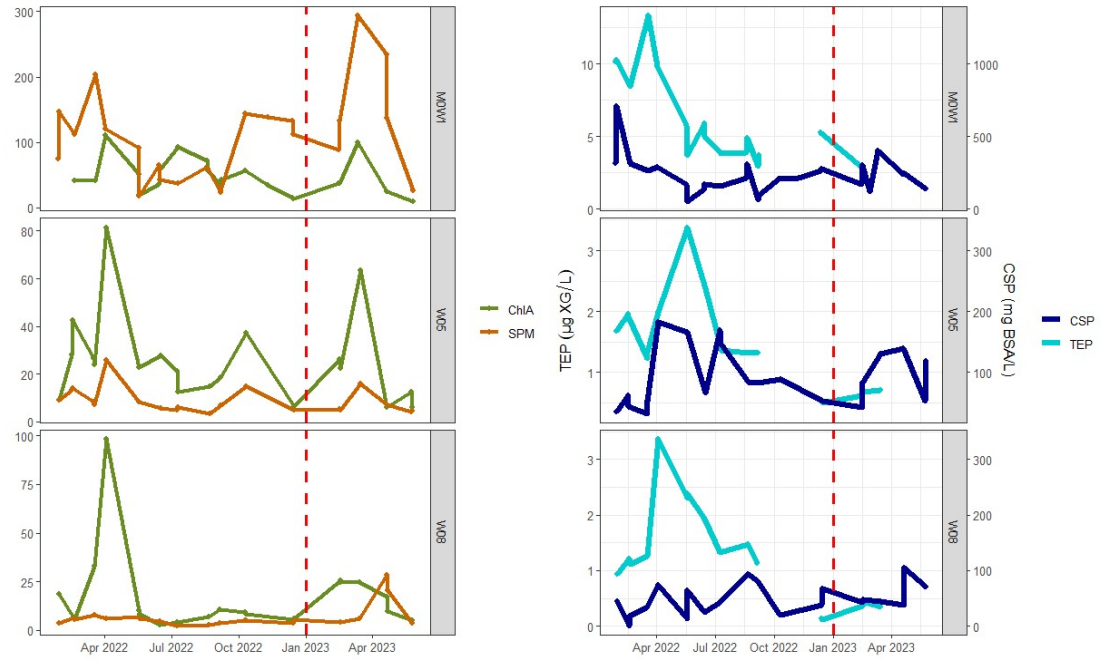

Figure 12: Left panels: concentration of chlorophyll a (µg/L) (green) and suspended particulate matter (SPM) (brown) (mg/L), average values (samples taken, processed by INS, data provided by INS) for the three stations. Right panels: spectrophotometrically determined concentration of CSP (mg BSA/L) (dark blue) and TEP (µg XG/L) (light blue), average values (samples taken and analysed respectively by UGent and by INS). Note the different scales between the subfigures. Red dashed line indicates the end of the year.

The TEP-microscopy concentration (total area of TEP, µm²/L) (Fig.13b) shows a minimum in summer in all 3 stations, although the pattern is strongest at the offshore station. Additionally, the values decrease with increasing distance from the coast. Furthermore, this summer decline arrives slightly earlier in the season at W08, and later on as we get closer to shore. Also the second peak occurs earlier offshore than inshore. The CSP-microscopy concentration (µm²/L, Fig.13b) shows a peak in winter at the coastal station, but much less strong patterns in the transition zone, and interestingly an opposite pattern at the offshore station. The transition zone has a slightly higher abundance of CSP during April (both years). The average particle surface area (~ size, µm²) (Fig.13a) follows the same patterns as the total area of particles for W05 and W08, but not for M0W1. It has been shown that TEP – like other organic components – is subject to interactions with mineral particles through adsorption and embedding due to ionic or Van der Waals interactions (Keil et al., 1994; Keil and Mayer, 2014). This results in TEP being separated into two distinct fractions: a mineral-associated fraction, considered more stable and less sticky, and a fresh fraction seen as more labile and more sticky (Fettweis et al., 2022). At MOW1, where mineral particles in suspension are very abundant, we expect to find mineral particles covered with mineral-associated TEP. The spectrophotometrically determined concentrations of TEP at MOW1 shows indeed a higher TEP concentration in winter and spring. The summer decrease in SPM concentrations induces a decrease of TEP concentration (Fig.12), and concomitantly we expect – based on Fettweis et al., 2022 – an increase in fresh, sticky TEP. The average size (in µm^2) of TEP at MOW1 (Fig.13a) illustrates this dynamics: it is higher in winter than in summer at the surface of the water column because large SPM particles and their mineral-associated TEP tend to settle to the bottom of the water column in the summer.

More generally, TEP and CSP concentrations (Fig.12) tend to show a maximum value in the winter-spring at MOW1 and in the spring at W05 (transition) and W08 (offshore).

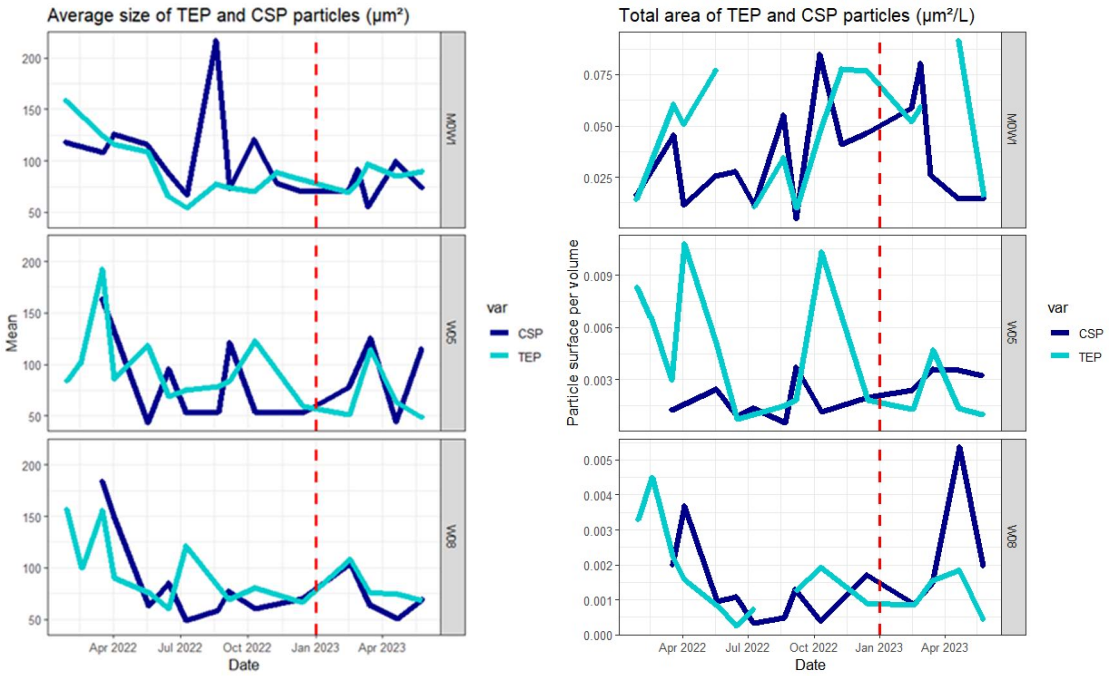

Figure 13: Average particle surface area (~ size) (left) and total surface of particles (right) for CSP (dark blue) and TEP (light blue) microscopic data. Red dashed line indicates the end of the year.

In the 1-100µm size fraction (I-FCM), the following small particle types were distinguished: particles containing microalgae (identified by chlorophyll autofluorescence) and particles containing other material (heterotrophs, bacteria, minerals…) (Fig.14). The particles without autofluorescence can be split into 2 categories: free living bacteria and particles colonized by bacteria. The particles containing autotrophs also contain 2 groups: healthy, free living phytoplanktonic cells and degraded and/or particle-attached phytoplanktonic cells (Fig.14). The abundance of particles without autotrophs more or less follows the pattern of the chlorophyll a concentration in MOW1 and MOW5 (figures 12, 15), which is interesting because these do not actually contain any chlorophyll a, and the SPM peak is in winter (although there is a local maximum in the winter as well, most notably at the transition zone and offshore station) (Fig.12). The reason of this discrepancy is as yet unknown. The free living bacteria seem to be most abundant in late spring and summer. Bacterial colonization (number of bacteria/µm² of particle) (Fig.16) of particles increases with season (maximum in summer) at the coastal station, but remains rather invariant in the other stations. The amount of particle attached phytoplankton is much higher at the coastal station, likely due to its high SPM concentration. Interestingly, we saw earlier that the chlorophyll a and the large cells abundance (FlowCam data) was higher in spring 2022 than spring 2023, and we notice here that the abundance of small phytoplanktonic cells was much higher in 2023.

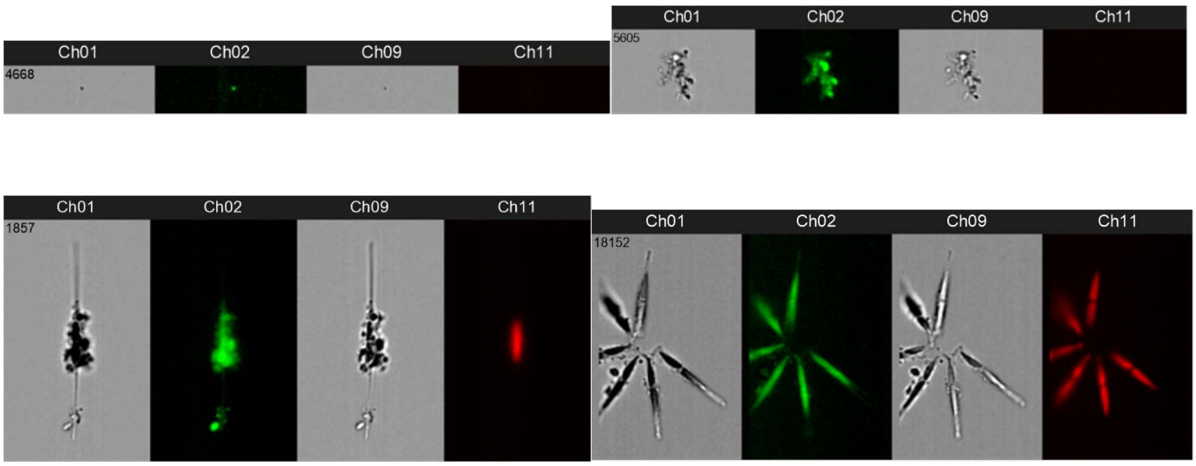

Figure 14: Example data acquired with imaging Flow Cytometry (iFCM). Channels indicate biological content of particles: Ch01 and Ch09 are Brightfield images at different focus depth, Ch02 is SybrGreen signal (DNA and RNA), Ch11 is autofluorescence signal (chloroplasts). Top row - particles without autotrophs <100µm: free living bacteria (left) & particles containing heterotrophs and/or mineral material colonised by bacteria (right). Bottom row - particles containing autotrophs <100µm: particles attached to and/or containing degraded phytoplankton (left) & free living, healthy phytoplankton (right).

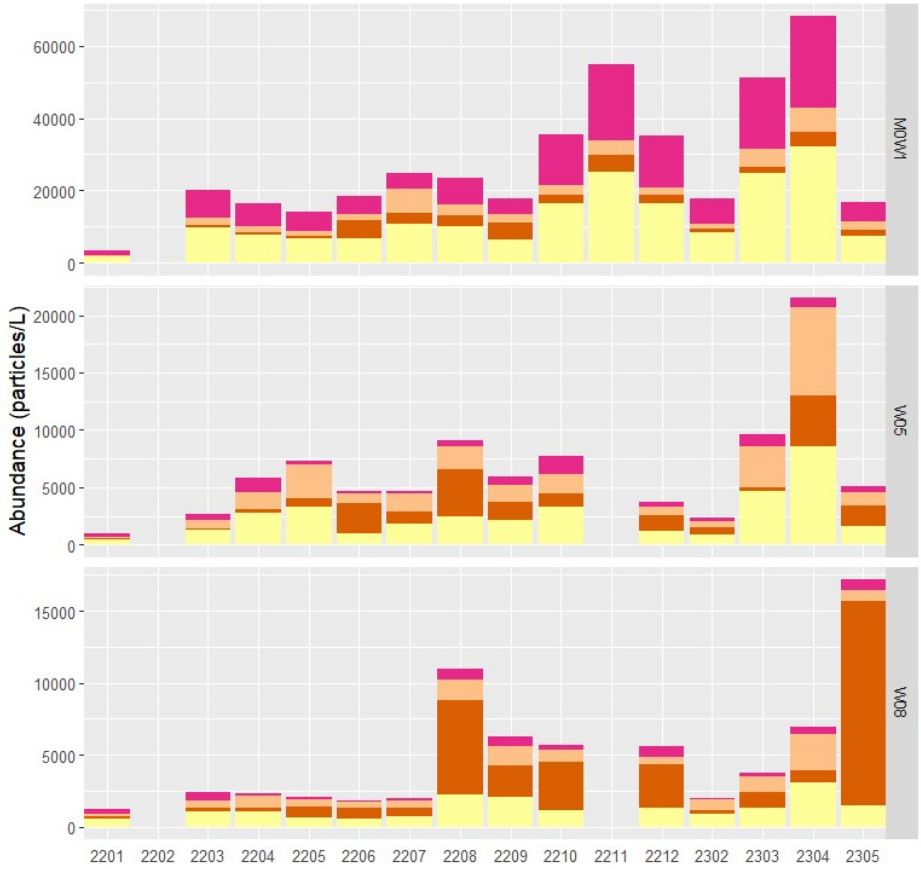

Figure 15: Abundance of particles <100µm (iFCM): pink: particle attached and/or degraded phytoplankton, beige: free living and/or healthy phytoplankton, brown: free living bacteria & yellow: particles containing heterotrophs and/or mineral material colonised by bacteria. The x-axis is date-coded as last 2 digits of the year + month number from January 2022 to May 2023. Red dashed line indicates the end of the year.

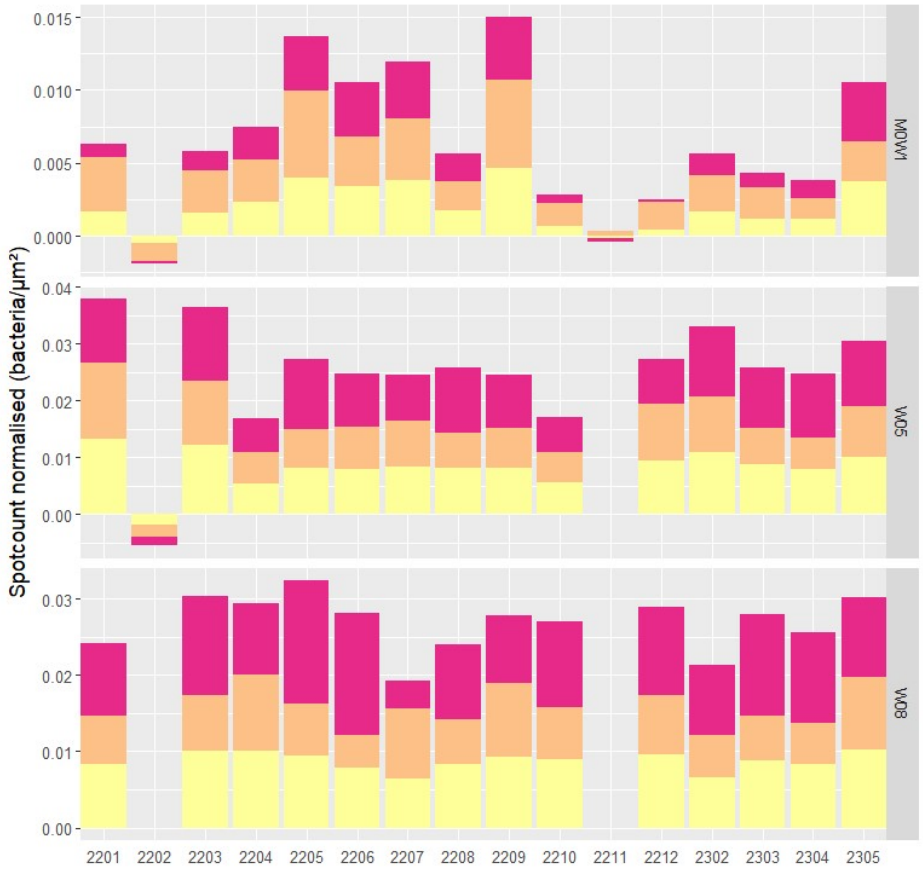

Figure 16: Bacterial colonisation of particles <100µm (iFCM): pink: particle attached and/or degraded phytoplankton, beige: free living and/or healthy phytoplankton & yellow: particles containing heterotrophs and/or mineral material. The x-axis is date-coded as last 2 digits of the year + month number from January 2022 to May 2023. Red dashed line indicates the end of the year.

The growth experiments (Fig.17) allow us to characterize the temperature – light niche of the abundant species of the studied area. We can see that *Rhizosolenia* sp. grows best at medium to high light, and within a temperature range of 12-18°C. In the other conditions, its growth is impeded (high variability between replicates, low regression slope) or even prevented entirely. From this we can best define the conditions in which to proceed with the marine gels production experiments; the selected conditions were 12°C/low light, 18°C/high light and as a control 15°C/medium light. Similar graphs were produced for the other species (data not shown).

The marine gel production experiments give us an insight under what conditions the dominant strains of the Belgian Part of the North Sea produce marine gels. Marine gels: dissolved sugars (Fig.18), TEP (Fig.19), CSP (Fig.20) production is highest during the stationary phase of the experiment, most likely because the cells are stressed by lack of nutrients in the medium. TEP production appears to be higher under high light condition (stress), but this has yet to be statistically validated. The dominant strains of the phytoplanktonic community not only participate differently to the marine gels production, but they perform differently under different conditions, and therefore physiological state. *Thalassiosira* sp., *Odontella* sp. and *Chaetoceros* sp. (all early to mid spring species) seem to have a constant sugar and TEP production rates, except under high light conditions. *Phaeocystis* sp. produces better in optimal conditions, while *Skeletonema* sp. and *Rhizosolenia* sp. show a high variability in their sugar and TEP production throughout their range (with a high rate of production for Rhizosolenia under medium light intensity and lower nutrient concentration).

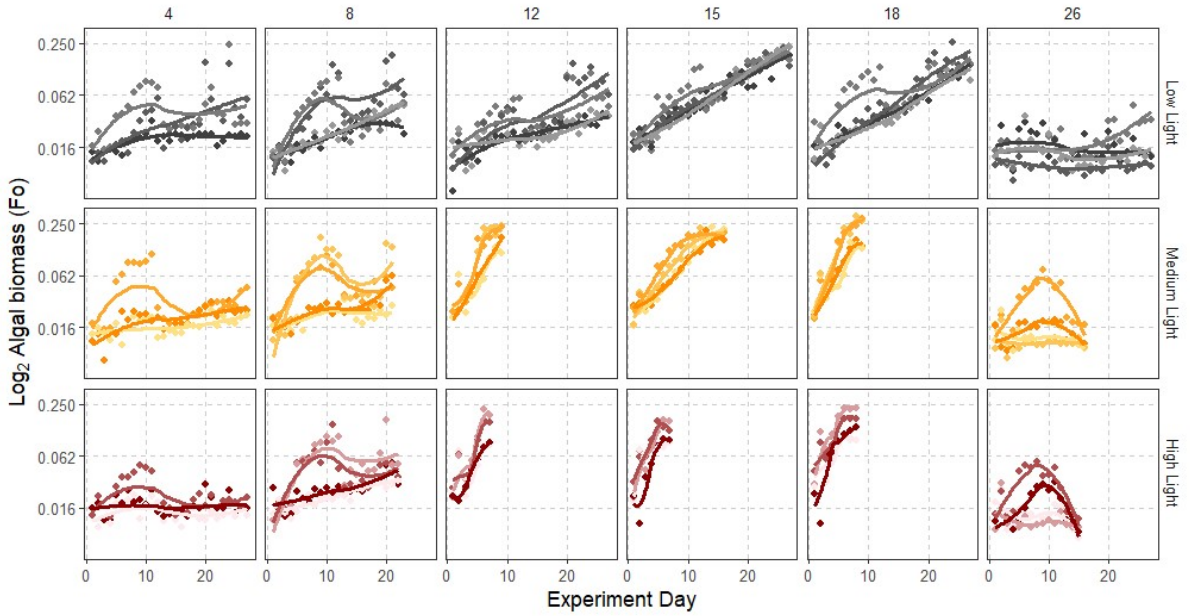

Figure 17: Growth experiment niche characterization for Rhizosolenia.

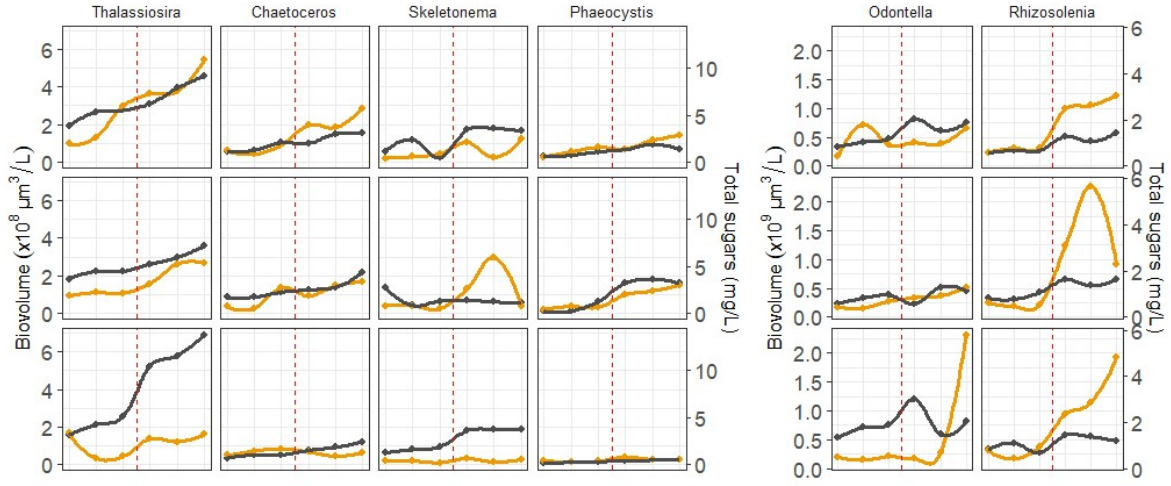

Figure 18: Production of total dissolved sugars (monosaccharides + polysaccharides)(orange) in comparison to the estimated biovolume (black) calculated on the basis of measured cell size and cell count (Hillebrand et al. 1999). X-axis is time in days (see Fig.17). Top to bottom illustrates low to high light conditions.

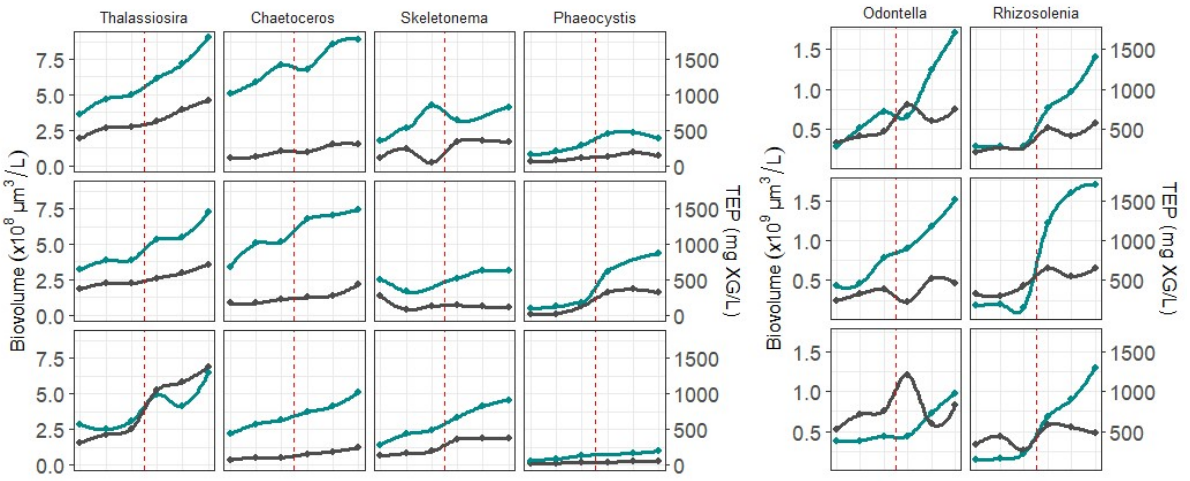

Figure 19: Production of TEP (blue) in comparison to the estimated biovolume (black) calculated on the basis of measured cell size and cell count (Hillebrand et al. 1999). X-axis is time in days (see Fig.17). Top to bottom illustrates low to high light conditions.

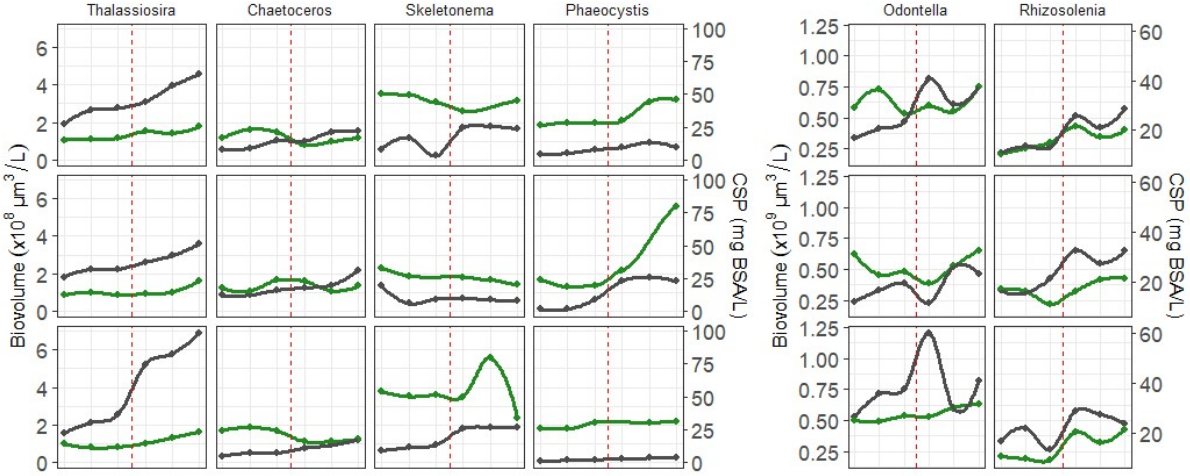

Figure 20: Production of CSP (green) in comparison to the estimated biovolume (black) calculated on the basis of measured cell size and cell count (Hillebrand et al. 1999). X-axis is time in days (see Fig.17). Top to bottom illustrates low to high light conditions.

1.4. Modeling the phytoplankton-sediment interactions

1.4.1. Introduction

Since the description of Transparent Exopolymer Particles (TEP) in the 1990s (Alldredge et al., 1993), their ecological significance has been increasingly recognized due to their high stickiness and ability to promote aggregation, affecting suspended particulate matter (SPM) dynamics and carbon cycling (Mari et al., 2017; Fettweis et al., 2022). However, few modelling studies have investigated the dynamics of Extracellular Polymeric Substances (EPS) and TEP and their effects on marine aggregation. On the one hand, biological model simulating EPS-TEP production slowly emerge (e.g., Kerimoglu et al., 2022). On the other hand, aggregation theory has been successfully applied to study diatom bloom fate and particle size spectra for example (Burd and Jackson, 2009). But biological and mineral particles are usually treated separately although the complex composition of flocs (including mineral and organic particles) is acknowledged (Ho et al., 2022). The BG-PART modelling work package addresses this gap by coupling the EPS-TEP production model of Kerimoglu et al. (2022) with the TCPBE mineral aggregation model of Lee et al. (2011). This integration marks a pioneering step in combining biological and mineral dynamics in biogeochemical models. We aim to investigate how EPS-TEP production influences SPM dynamics and turbidity, how changes in turbidity affect phytoplankton growth, and the extent to which phytoplankton can alter its environment through EPS production.

1.4.2. Methods

This section briefly presents the two existing models that are coupled (Sections 1.4.2.1 and 1.4.2.2) and their coupling and implementation at station MOW1 in the Belgian coastal zone (Section 1.4.2.3). The optimization procedure used for this new application is described in Section 1.4.2.4.

1.4.2.1. The plankton ecosystem model including EPS-TEP production

The biological model used as basis for this study is the intermediate-complexity (27 state variables) numerical model of Kerimoglu et al. (2022). It describes the dynamics of nutrients (N, P, Si), diatoms, small and large dissolved organic matter (DOM), TEP, small and large detritus, two bacterial communities, and two heterotrophic protists (flagellates and ciliates). Fig. 21a shows the diagram representing the state variables and the fluxes through which they interact. Phytoplankton exudation leads to the production of DOM (functionally equivalent to EPS in the model) that leads to the production of TEP through aggregation (coalescence “C” in Fig. 21a). TEP loss terms include aggregation (flocculation “F” in Fig. 21a) into large detritus and ingestion by attached bacteria, heterotrophic flagellates and ciliates. The model simulated a mesocosm seeded with plankton assemblages from the coastal North Sea and forced with nutrient, temperature and light conditions reflecting the natural conditions, constituting an appropriate basis for the current application in Belgian waters.

1.4.2.2. The mineral aggregation model

The mineral aggregation model used in this study is the TCPBE model of Lee et al. (2011). In this model, the bimodal sediment size distribution observed in coastal waters is simulated through the representation of size-fixed microflocs and size-varying macroflocs. Fig. 21b shows the simulated processes in a Petersen matrix displaying how the different processes (rows) affect the components of the system (columns; i.e., the three state variables): macroflocs can be produced from the collision of microflocs, of microflocs and macroflocs, or of macroflocs (aggregation); in turn, they can break down into micro- and macroflocs (breakage). Aggregation is not only a function of the collision

frequency (which depends on the size of the particles), but also of the collision efficiency α which determines the fraction of collisions that result in actual aggregation. This model has been successfully applied to the Belgian coastal waters to simulate SPM dynamics during tidal cycles (Lee, pers. comm.)

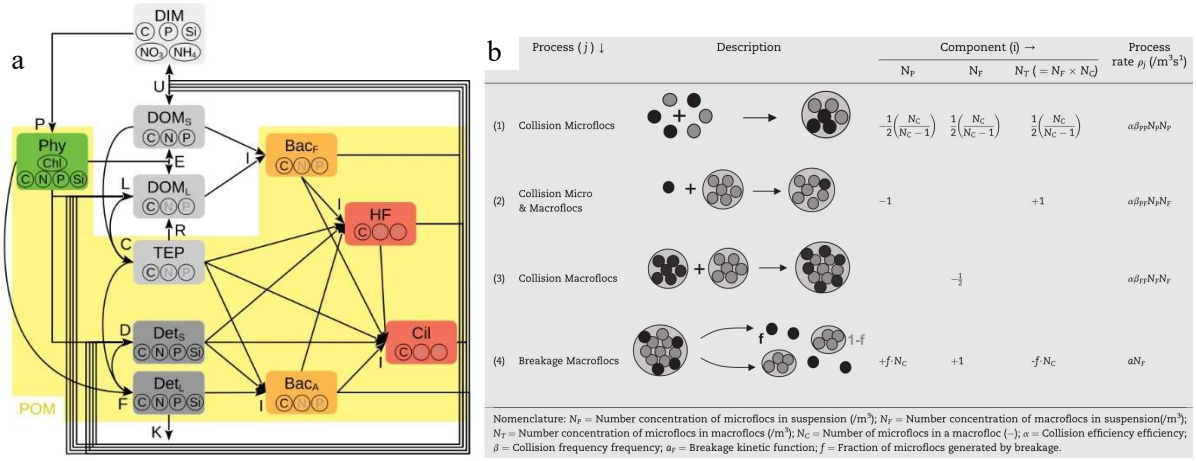

Fig. 21. The biogeochemical model of Kerimoglu et al. (2002; a, left) and the mineral aggregation model of Lee et al. (2011; b, right) which are coupled in this study. See original publications for details.

1.4.2.3. Coupling the biological and mineral models, and implementation in the BCZ

The biological model of Kerimoglu et al. (2022; Section 1.4.2.1) and the mineral flocculation model of Lee et al. (2011; Section 1.4.2.2) are here coupled. Freshly produced TEP enhances mineral particle flocculation through its stickiness, in turn affecting SPM dynamics (Fettweis et al., 2022; Desmit et al., 2024). This is translated by making the collision efficiency of macroflocs interactions proportional to TEP:

$$\alpha_{FF} = \alpha_{ref} \times \sqrt{TEP} \qquad \text{(Eq. 1)}$$

where α_{ref} is the reference collision efficiency in the flocculation model and TEP is the TEP concentration in the biological model. With this modification, collision efficiency for macroflocs vary between 0.02 and ~0.08 depending on the biological activity and TEP concentrations. In addition, a settling loss for macroflocs is introduced according to a modified Stokes's law where the settling rate w_s is dependent on the floc diameter $diam_F$:

$$w_s = \frac{2000}{9} \times (\rho_F - \rho_{water}) \times g \times \frac{{diam_F}^2}{n} \qquad \text{(Eq. 2)}$$

where ρ_{water} and ρ_F are the densities of water and of flocs respectively (i.e., 1000 kg m^{-3} and 1200 kg m^{-3} respectively), g is the gravitational acceleration (9.81 m s^{-2}) and n is the water dynamic viscosity (10^{-3} Ns m^{-2}). Finally, feedback on biological activity is incorporated in the model through the addition of light attenuation by mineral flocs in the water column. Following the methodology of Tian et al. (2009), the extinction coefficient K_d is calculated as a composite value, summing the light extinction caused by living organisms, detritus, and the newly included macroflocs concentration:

$$K_d = \sum_j \varepsilon_j \times [j] + \varepsilon_F \times \sqrt{[F]} \quad \text{(Eq. 3)}$$

where ε_j and $[j]$ are respectively the specific light attenuation coefficients and the concentrations of the different tracers affecting light in the water column ($j = \{Diatoms,\ Detritus,\ Bacteria,\ Flagellates,\ Ciliates\}$; see values in Kerimoglu et al., 2022), and ε_F and $[F]$ are respectively the specific light attenuation coefficient and the concentration of macroflocs.

The coupled biological-mineral model is implemented in a 0D homogeneous box representing station MOW1 in the Belgian coastal zone. The simulation focuses on the early season dynamics, beginning on February 1st until April 30th to capture the onset and development of the spring diatom bloom. Initial concentrations of nutrients and organisms are based on observed values collected by BG-PART and the BGC-Monit program. In situ photosynthetically active radiation is used to provide a light regime with diurnal and seasonal variation.

Some parameters were calibrated to ensure the model performs well in this new implementation, as explained in the next section.

1.4.2.4. Optimization implemented for parameter calibration

Model parameters related to diatom physiology and organic matter aggregation were calibrated against observations in the Belgian coastal zone. A 1-year climatology of observations was used for Chl a, NH4, NO3, dissolved inorganic P (DIP), dissolved inorganic Si (DSi), diatom carbon biomass, and fresh TEP carbon at station MOW1. TEP is measured in mg xanthan gum equivalent l-1, converted to fresh TEP carbon using a factor of 1 mgC l-1 ~ 0.55 mgXGeq l-1 (Fettweis et al., 2022). Differential Evolution was used for calibration, known for robustness and parallelization (Storn and Price, 1997). Control variables were set to speed up optimization: parameter vectors' population size was 105, weighting factor was 0.5, and crossover constant was 0.9. The optimization criterion was maximum log-likelihood, assuming normal distribution of model-observations residuals.

1.4.3. Results and Discussion

In this section we show the model results for two setups: the uncoupled setup (working with the biological module only) and the coupled setup (biological and flocculation modules). Fig. 22 shows the time evolution of the diatom concentration in carbon biomass (Fig. 22a), Chl *a* (Fig. 22b), nutrients (Fig. 22e, f, i, j), TEP (Fig. 22c), components of the mineral particles (Fig. 22d, h, l), floc diameter (Fig. 22g) and floc settling velocity (Fig. 22k) over the simulated periods (Feb-Apr) in comparison to observations (used for calibration) when available.

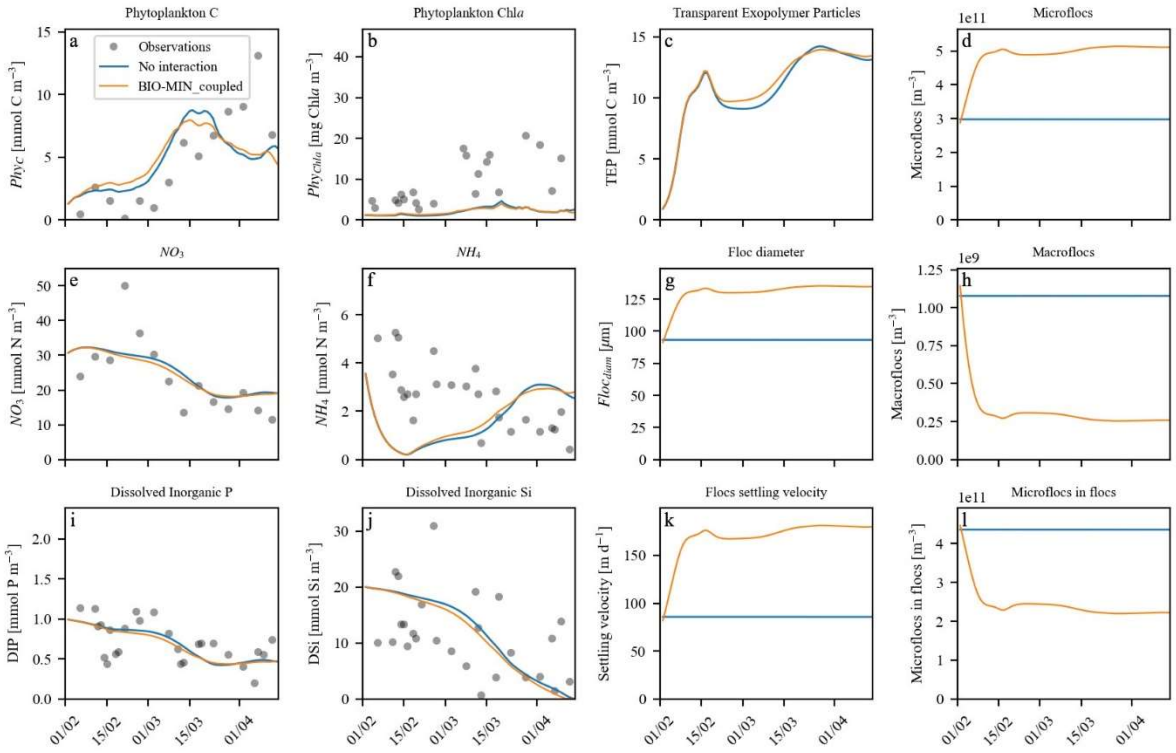

Fig. 22. Model results in the uncoupled (blue) and coupled (orange) simulations. Dots are in situ observations at MOW1.

The timing and extent of the diatom bloom (Fig. 22a) is well caught by the model. Although the trend and timing of the Chl *a* evolution (Fig. 22b) are correct, the model underestimates Chl *a* levels by a factor ~5 (likely related to a model parameterization or formulation which is currently under investigation). Nutrients (Fig. 22e, f, I, j) are properly caught by the model, with the typical decrease from winter elevated concentrations to lower levels following their uptake by phytoplankton, which can lead to nutrient limitation (especially DSi and, to some extent, DIP in this eutrophied area; Lancelot et al., 2005; Billen et al., 2011; Desmit et al., 2018). The production of fresh TEP accompanies the diatom bloom (Fig. 22c), which enhances the aggregation of macroflocs in the coupled version (see Section 1.4.2.3). As a result, the number of macroflocs decreases in the coupled model (orange, Fig. 22h) while their diameter increases (Fig. 22g), indicating that the flocs become larger and less numerous. Additionally, their settling velocity increases alongside their diameter with a doubling (from ~80 m d^{-1} to ~160 m $d^{-}1$; Fig. 22k; Eq. 2 in Section 1.4.2.3), resulting in greater losses for macroflocs. Overall, this leads to a decline in floc abundance throughout spring as fresh TEP levels rise, consistent with observations in this area (Fettweis et al., 2022).

The model can be used to investigate the feedback effect of the mineral macroflocs on the biological component of the system: the varying floc concentration will affect the light regime experienced by diatoms in the water column (Eq. 3 in Section 1.4.2.3). The comparison of the diatom biomass (Fig. 22a) between the two simulations shows that their seasonal evolution is affected over the whole simulated period. At the onset of the bloom in early February, when light is limiting, decreased floc concentration leads to higher light available for growth and earlier blooms developments (i.e., the orange diatom biomass increases faster than the blue one in February). Yet, the peak level reached at the maximum of the bloom later in March is lower. Further investigation indicated that faster growth in the coupled simulation is mostly due to higher primary production (with reduced floc

concentration and increased light regime), but that larger loss due to aggregation later on in the coupled simulation explains the lower bloom concentrations and earlier decline.

1.4.4. Conclusions and Perspectives

The coupled biological-mineral model successfully simulates key features of the Belgian coastal zone, such as the spring diatom bloom and the reduction in floc concentrations from their winter maximum. By coupling plankton and organic matter dynamics with mineral flocculation dynamics, this model offers a novel tool for investigating complex organo-mineral interactions with unprecedented detail and realism. While refinements are needed, it already shows that biological-mineral interactions significantly impact coastal water tracers and improve biogeochemical models. Specifically, plankton-mediated flocculation and floc sedimentation notably influence diatom dynamics. Planned BG-PART lab experiments investigating the TEP-bacteria-zooplankton interactions will enable the improvement of the TEP and floc cycle representation in the model. Additionally, ongoing BG-PART experiments aim to investigate the diversity in diatom ecophysiology and TEP production in Belgian waters: the additional info can be incorporated into the model building on diversity-based studies like Terseleer et al. (2014). Furthermore, floc composition, which includes both organic and mineral compounds (as observed in BG-PART and reviewed in Ho et al., 2022), is currently modelled as separate detritus and minerals. The next development step is to integrate these into a homogeneous floc variable, improving simulations of mixed organic-mineral particles. Once implemented in 0D or 1D-vertical models in North Sea areas, or the 3D COHERENS model, this biological-mineral model will be a pioneering tool from BG-PART for studying SPM dynamics and carbon cycling.

Literature

Alldredge, A. L., Passow, U., & Logan, B. E. (1993). The abundance and significance of a class of large, transparent organic particles in the ocean. Deep Sea Research Part I: Oceanographic Research Papers, 40(6), 1131-1140.

Billen, G., M. Silvestre, B. Grizzetti, and others. 2011. Nitrogen flows from European watersheds to coastal marine waters, p. 271–297. In The European nitrogen assessment : sources, effects, and policy perspectives. Sutton, M. A. (ed.), Cambridge University Press. ISBN 9781107006126.

Burd, A. B., & Jackson, G. A. (2009). Particle aggregation. Annual review of marine science, 1(1), 65-90.

Desmit, X., Schartau, M., Riethmüller, R., Terseleer, N., Van der Zande, D., Fettweis, M., 2024. The transition between coastal and offshore areas in the North Sea unraveled by suspended particle composition. Science of The Total Environment 915, 169966. https://doi.org/10.1016/j.scitotenv.2024.169966

Desmit, X., Thieu, V., Billen, G., …, Lacroix, G., 2018. Reducing marine eutrophication may require a paradigmatic change. Science of The Total Environment 635, 1444–1466. https://doi.org/10.1016/j.scitotenv.2018.04.181

Fettweis, M., Schartau, M., Desmit, X., Lee, B. J., Terseleer, N., Van der Zande, D., ... & Riethmüller, R. (2022). Organic matter composition of biomineral flocs and its influence on suspended particulate matter dynamics along a nearshore to offshore transect. Journal of Geophysical Research: Biogeosciences, 127(1), e2021JG006332.

Ho, Q. N., Fettweis, M., Spencer, K. L., & Lee, B. J. (2022). Flocculation with heterogeneous composition in water environments: a review. Water Research, 213, 118147.

Kerimoglu, O., Hintz, N. H., Lücken, L., Blasius, B., Böttcher, L., Bunse, C., ... & Simon, M. (2022). Growth, organic matter release, aggregation and recycling during a diatom bloom: a model-based analysis of a mesocosm experiment. bioRxiv, 2022-05.

Lancelot, C., Y. Spitz, …, and G. Billen. 2005. Modelling diatom and *Phaeocystis* blooms and nutrient cycles in the Southern Bight of the North Sea: The MIRO model. Mar. Ecol. Prog. Ser. 289: 63–78. doi:10.3354/meps289063

Lee, B. J., Toorman, E., Molz, F. J., & Wang, J. (2011). A two-class population balance equation yielding bimodal flocculation of marine or estuarine sediments. Water research, 45(5), 2131-2145.

Storn, R., & Price, K. (1997). Differential evolution–a simple and efficient heuristic for global optimization over continuous spaces. Journal of global optimization, 11, 341-359.

Terseleer, N., Bruggeman, J., Lancelot, C., & Gypens, N. (2014). Trait-based representation of diatom functional diversity in a plankton functional type model of the eutrophied southern North Sea. Limnology and Oceanography, 59(6), 1958-1972.

Tian, T., Merico, A., Su, J., Staneva, J., Wiltshire, K., & Wirtz, K. (2009). Importance of resuspended sediment dynamics for the phytoplankton spring bloom in a coastal marine ecosystem. Journal of Sea Research, 62(4), 214-228.

2. Preliminary Conclusions

At this stage, all principal investigators (PI) in the project are well aware of the results obtained by each other in the consortium. Data exchange is intense between the three institutes involved, and with institutes abroad. When needed, additional datasets are extracted from colleague remote sensing and modeling communities.

All PIs have been asked to prepare a first draft paper by the end of October 24 with their own results. The objective – beside the publication – is that each PI re-order and presents his/her results in a fine way to prepare the transdisciplinary analysis and to feed the model parameters with as many lab/field values as possible.

The winter-spring period will be used to gather the results and elaborate together a transdisciplinary analysis. For six months already, we have intensified the online discussions to prepare such analysis.

3. Future Prospects and Planning

Particle dynamics

Most of the objectives are reached. We are refining our analysis with inputs from Belspo-funded project PiNS with a focus on their mineralogical analysis. One objective is to link our findings on particle dynamics with the carbon cycle.

Phytoplankton succession

The above-shown community composition data will be compiled from the FlowCam and iFCM data (UGent), the flow cytometry data (VLIZ) and an eDNA metabarcoding dataset that was additionally produced by PAE-UGent (not funded by BG-Part).

Zooplankton succession and ecological function

Some small grazing experiments will be set up in the third quarter of 2024 to stress test the setup and cultivate lab skills. Full blown grazing experiments are foreseen in the last quarter 2024.

Phytoplankton niches and marine gel production

The samples taken for chlorophyll a and C:N during the marine gels production experiments still need to be processed (before end of 2024). These results are also directed to feed the modeled processes and parameters (WP4).

Modeling

Some refinements are planned in the model to improve the processes and the parameter values. The model must be applied at three different sites along the cross-shore gradient (MOW1, W05, W08). These sites subject to different conditions that have been measured during the project.

Transdisciplinary analysis

A transdisciplinary analysis addresses the remaining questions of the project. Immediate objectives: 1/ Establishing a landscape of phyto- and zooplankton succession in the coastal-offshore gradient; 2/ Linking the experimental data on TEP production to the occurrence patterns of the species in the Belgian waters and the concentration of marine gels found in the water column; 3/ Modeling the observed patterns in a simulated water column at the three sites.

4. Valorization

Publications

1. Desmit, X., Schartau, M., Riethmüller, R., Terseleer, N., Van der Zande, D., Fettweis, M., 2024. The transition between coastal and offshore areas in the North Sea unraveled by suspended particle composition. Science of The Total Environment 915, 169966. https://doi.org/10.1016/j.scitotenv.2024.169966

Workshop on Pelagic Particle Dynamics

The Workshop was held in October 4-6, 2023 at RBINS, Vautier Street 29, 1000 Brussels.

A manuscript is currently in preparation based on the Workshop discussions.

Conferences

1. Kallend, A., Dujardin, J.H., Fettweis, M., Vyverman, W., De Rijcke, M., Sabbe, K., Desmit, X., 2023. Interactions between phytoplankton, marine gels and suspended particulate matter in a dynamic, shallow coastal system before and during the phytoplankton spring bloom (Poster). Presented at the ASLO Aquatic Sciences Meeting, 4-9 Jun, Palma De Mallorca, Spain.

2. Kallend, A., Amadei Martinez, L., Debusschere, M., Skouroliakou, D.-I., Fettweis, M., Desmit, X., Vyverman, W., Sabbe, K., 2024. Light-temperature niche in North Sea phytoplankton : Potential implications of changing environment pressures on phytoplankton seasonal succession and marine gels production. Presented at the 57th European Marine Biology Symposium (EMBS), 16-20 Sep, Naples, Italy.

3. Terseleer, N., Fettweis, M., Silori, S., Desmit, X., Kallend, A., Amadei Martinez, L., Sabbe, K., Vyverman, W., Lee, B.J., Kerimoglu, O., 2024. A coupled phytoplankton-flocculation model to quantify suspended particulate matter dynamics on the Belgian shelf. Presented at the AMEMR 2024 Conference, 8-11 July, Plymouth, UK.

5. Follow-Up Committee

After the Workshop we held in Brussels in Oct 2023, the members of the Follow-Up Committee have been invited to participate to different manuscripts in preparation. We think that they can overview our work during the analysis phase, and contribute by being co-authors in the writing phase.

6. Problems and Solutions

Issue 1

The flow-through design of VLIZ's FRRF is non-standard, complicating data analyses. Rather than dark-incubating the sample prior to measurement to establish a baseline fluorescence F_0, this particular device measures the induction of fluorescence at different levels of ambient light, provided by an external light source. The external light comes with its own cycle/program and data output, which – for unknown reason - is adding incorrect timestamps to the data. Aligning the FRRF data with the data of the external light is proving challenging. We will seek help from FRRF users at the Royal Netherlands Institute for Sea Research (NIOZ) that co-designed the VLIZ setup.